Neutron star deformability with hyperonization in density-dependent relativistic mean-field models

W. Z. Shangguan,[1,2,†] Z. Q. Huang,[2] S. N. Wei,[1] and W. Z. Jiang[1,*]

[1]*School of Physics, Southeast University, Nanjing 211189, China*

[2]*Faculty of Pharmacy, GuangXi University of Chinese Medicine, Nanning 530200, China*

(Received 30 January 2021; accepted 19 August 2021; published 20 September 2021)

Neutron star tidal deformability extracted from gravitational wave data provides a novel probe to the interior neutron star structures and the associated nuclear equation of state (EOS). Instead of the popular composition of nucleons and leptons in neutron stars, we include hyperons and examine the role of hyperons in the tidal deformability and its impact on the symmetry energy in a relativistic mean-field approach with the density-dependent parametrizations. The hyperons are found to have a significant impact on the deformability, correlated sensitively with the onset density and fraction of hyperons in neutron star matter. A moderately lower onset density of hyperons can yield considerable modification to the tidal deformability and shift its inference on the nuclear EOS. The future measurements of the tidal deformability at multifiducial star masses are anticipated to lift the degeneracy between the contributions from the hyperon component and symmetry energy.

DOI: 10.1103/PhysRevD.104.063035

I. INTRODUCTION

According to the general relativity, the moving body changes the surrounding geometry, and the reciprocal motion or transient mass-change process can cause the sonic propagation of space-time oscillation, the so-called gravitational wave. The massive celestial binary merger is one of the strongest sources of gravitational waves. It was fascinating that the gravitational wave signal from the GW170817, which is a neutron star merger with a chirp mass 1.188 $M_\odot$ and 40 Mpc away from the Earth, was successfully detected by Ligo and Virgo detectors [1,2] more than 3 years ago. It is a historic event in the deep-sky detection. Its significance also exists in nuclear physics. Since then, the study on neutron stars heads into a multimessenger era. The tidal deformability measures the size of neutron stars and is correlated with the neutron distribution of heavy nuclei [3,4]. In particular, during the inspiral of the binaries close to merger, the tidal deformability of neutron stars encodes the information of the equation of state (EOS) of asymmetric matter in the interior neutron star.

The tidal deformability (or, alternatively the Love number) of neutron stars can be derived as a metric perturbation in the general relativity [5–7], since matter is the source of the metric. It was found that the Love number of normal neutron stars is quite different from that of strange quark matter stars [8,9]. Several research groups have engaged in exploring the tidal deformability with its possible constraint on the EOS of asymmetric matter. The uncertainty of the symmetry energy at saturation density just has a moderate effect on the tidal deformability [10]. Recently, the tidal deformability from the experiments is optimistically used to constrain the symmetry energy at suprasaturation densities [11,12].

Among all non-nucleonic degrees of freedom in neutron stars, the hyperon is an important but contentious ingredient. Usually, the inclusion of hyperons can clearly soften the nuclear EOS and reduce the maximum mass of neutron stars significantly, for instance, see Refs. [13,14]. It was even claimed that the observations of large-mass neutron stars (for instance, pulsars J1614-2230 [15] and J0740 + 6620 [16]) seem to rule out the hyperon EOS. On the other hand, quite a few hyperon EOSs were proposed to reproduce the 2 $M_\odot$ neutron stars [17–22]. One of the authors and his collaborators also worked out the hyperon EOS that is compatible with the mass and meantime the radius constraints of neutron stars [13] and is in the rank of fine models, see Ref. [23] and references therein. In spite of the dispute of the existence problem, the onset densities of hyperons and their fractions also diversify rather largely in a variety of models. These issues are rooted in the in-medium interactions for hyperons and remain largely unsolved. In a multimessenger era, the gravitational wave signals would hopefully light the secrets for the hyperon component in stars and the underlying interactions, although no much attention has been paid to the accordance between the available hyperon EOSs and the tidal deformability of the 1.4 $M_\odot$ stars for simplicity or due to the

*Corresponding author.
wzjiang@seu.edu.cn

†Visiting scholar at the first affiliation since the year of 2020.

absence of the hyperon involvement in extracting the EOS of asymmetric matter from terrestrial experiments. However, the seemly small chirp mass ($1.188\,M_\odot$) of the GW170817 with the component masses ranging from 1.17 to $1.6\,M_\odot$ does not ever mean that the hyperon component is negligible. In this work, we will aim to scrutinize the interplay between the tidal deformability and the hyperon EOS based on the previous density dependent relativistic mean-field (RMF) models [24,25]. In order to single out the hyperon effect beyond saturation density, we need first pin down the EOS in the low density region where there is a transition from the interior homogeneous phase to inhomogeneous crustal phase. We will determine the transition density by the instability condition of uniform matter [26,27] and further distinguish the inner and outer crusts by appropriately choosing different EOSs for the inner and outer crusts [28]. With moderately tuned onset densities and fractions of hyperons, we can observe the significant role of hyperons in affecting the tidal deformability of intermediate-mass neutron stars and the extraction of nuclear symmetry energy beyond saturation density.

The remainder of the paper is organized as follows. In the subsequent section, a brief formalism is presented for the differential equation of the Love number integrated in the Tolman-Oppenheimer-Volkoff (TOV) equation and the RMF EOS. The emphasis is placed on the corresponding parametrization of nuclear EOS concerning the hyperon interactions. In Sec. III, we present numerical results and analyze the hyperon effect on the tidal deformability and the nuclear EOS. Finally, a brief summary is given in Sec. IV.

II. FORMALISM AND PARAMETRIZATIONS

The quadrupole tidal field can be incorporated in the spacetime metric as an external perturbation specified by a function H which satisfies the following differential equation [6]:

$$H''(r)+\left[\frac{2}{r}+e^{\lambda(r)}\left(\frac{2M(r)}{r^2}+4\pi r(p(r)-\mathcal{E}(r))\right)\right]\times H'(r)+H(r)Q(r)=0, \tag{1}$$

where

$$Q(r)=4\pi e^{\lambda(r)}\left(5\mathcal{E}(r)+9p(r)+\frac{d\mathcal{E}(r)}{dp(r)}(p(r)+\mathcal{E}(r))\right)-6\frac{e^{\lambda(r)}}{r^2}-(\nu'(r))^2, \tag{2}$$

and the metric functions $\lambda(r)$ and $\nu(r)$ are given as

$$e^{\lambda(r)}=\left[1-\frac{2M(r)}{r}\right]^{-1},\qquad \nu'(r)=2e^{\lambda(r)}\frac{M(r)+4\pi r^3p(r)}{r^2}, \tag{3}$$

with $M(r)$, $p(r)$, and $\mathcal{E}(r)$ being the mass, pressure, and energy density, respectively. By redefining the quantity $y=H'/H$, Eq. (1) turns out to be the following first-order differential equation:

$$y'(r)+y^2(r)+F(r)y(r)+Q(r)r^2=0, \tag{4}$$

where

$$F(r)=e^{\lambda(r)}[1+4\pi r^2(p(r)-\mathcal{E}(r))], \tag{5}$$

with $y(0)=2$. The Love number k_2 is obtained at the neutron star surface with $y_R=y(R)$, and it is given by

$$\begin{aligned}k_2(y_R)=&\frac{8}{5}\beta^5(1-2\beta)^2[2-y_R+2\beta(y_R-1)]\{2\beta\\&\times[6-3y_R+3\beta(5y_R-8)]+4\beta^3[13-11y_R\\&+\beta(3y_R-2)+2\beta^2(1+y_R)]+3(1-2\beta)^2\\&\times[2-y_R+2\beta(y_R-1)]\ln(1-2\beta)\}^{-1},\end{aligned} \tag{6}$$

where $\beta=M/R$ is the dimensionless compactness parameter in units of $G=c=1$. The tidal deformability is given by

$$\Lambda_g=\frac{2}{3}k_2\left(\frac{R}{M}\right)^5, \tag{7}$$

with R and M being the radius and mass of the neutron star, respectively.

Equation (4) for the perturbation tidal field should be solved together with the TOV equations:

$$p'(r)=-\nu'(r)[p(r)+\mathcal{E}(r)]/2,\qquad M'(r)=4\pi r^2\mathcal{E}(r), \tag{8}$$

which are solved by integrating over the radial coordinate from the star center to the surface where the pressure vanishes. We perform the integration with the fourth-order Runge-Kutta method. The nuclear EOS, i.e., $p(\mathcal{E})$ is an input of the integration. The central energy density or pressure is chosen as a free parameter to obtain a mass-radius trajectory for neutron stars.

In obtaining the deformability, the conveniently and popularly used method relies on the EOS with a simple neutron star composition of nucleons and leptons or a polytropic piecewise EOS, whereas we start the work from a Lagrangian that consists of the fields of baryons, leptons (e, μ), and mesons, and the interactions between them. Here, we invoke directly the energy density and pressure from the previous density-dependent RMF models [13]:

$$\mathcal{E} = \frac{1}{2}m_\omega^{*2}\omega_0^2 + \frac{1}{2}m_\rho^{*2}b_0^2 + \frac{1}{2}m_\phi^2\phi_0^2 + \frac{1}{2}m_\sigma^{*2}\sigma^2 + \frac{1}{2}m_{\sigma^*}^2\sigma^{*2} + 2\sum_i \int_0^{k_{Fi}} \frac{d^3k}{(2\pi)^3} E_i^*, \tag{9}$$

$$p = \frac{1}{2}m_\omega^{*2}\omega_0^2 + \frac{1}{2}m_\rho^{*2}b_0^2 + \frac{1}{2}m_\phi^2\phi_0^2 - \frac{1}{2}m_\sigma^{*2}\sigma^2 - \Sigma_0^R\rho - \frac{1}{2}m_{\sigma^*}^2\sigma^{*2} + \frac{2}{3}\sum_i \int_0^{k_{Fi}} \frac{d^3k}{(2\pi)^3}\frac{\mathbf{k}^2}{E_i^*}, \tag{10}$$

where i runs over the species of baryons and leptons considered in neutron star matter, $E_i^* = \sqrt{\mathbf{k}^2 + m_i^{*2}}$ with m_i^* being the Fermion effective mass, and Σ_0^R is the rearrangement term, originated from the density-dependent parameters. The explicit formula of the rearrangement term can be referred to Ref. [29]. The meson coupling constants and masses with asterisks denote the density dependence, given by the Brown-Rho scaling functions [13,24,25]. It is interesting to note that the parametrization with this density dependence respects the chiral limit in terms of the vanishing scalar density and nucleon effective mass at high densities, which is interpreted as the vector manifestation of chiral symmetry in the hidden local symmetry theory [30]. In the present work, the RMF parameter sets SLC and SLCd [13,25] that can reproduce the ground-state properties of finite nuclei and meet the 2 $M_\odot$ constraint of neutron stars are adopted to study neutron stars with hyperonization, and the composition of neutron stars consists of baryons $(N, \Lambda, \Sigma, \Xi)$ and leptons (e, μ).

For the hyperonic sector, the strange mesons ϕ (1020 MeV) and σ^* (i.e., f_0, 975 MeV), in addition to normal mesons, are included with their parameters free of density [13]. The coupling of hyperons with normal mesons can generally be specified by the ratios of the meson coupling with hyperons to that with nucleons: $X_{iY} = g_{iY}/g_{iN}$ with i denoting meson species. Although these ratio parameters are, in most cases, taken to be constants in the literature, they are being density-dependent ones $X_{iY}(\rho)$ for the scaling functions for hyperons [13]:

$$\begin{aligned}
\Phi_{\omega\Lambda(\Sigma)}(\rho) &= \left(\frac{1}{3} - \alpha\right)\Phi_{\omega N}(\rho_0) + \left(\frac{2}{3} + \alpha\right)\Phi_{\omega N}(\rho), \\
\Phi_{\omega\Xi}(\rho) &= \left(\frac{2}{3} - \alpha\right)\Phi_{\omega N}(\rho_0) + \left(\frac{1}{3} + \alpha\right)\Phi_{\omega N}(\rho), \\
\Phi_{\sigma Y}(\rho) &= (1 - f_{\sigma Y})\Phi_{\sigma N}(\rho_0) + f_{\sigma Y}\Phi_{\sigma N}(\rho),
\end{aligned} \tag{11}$$

where $\Phi_{iN}(\rho)$ are the nucleon scaling functions, ρ_0 is the saturation density (0.16 fm^{-3}), and $f_{\sigma Y}$ and α are adjustable constants. The scaling function $\Phi_{\rho\Xi}$ for the ρ meson takes the same as that of the ω meson. The product of the free-space meson-baryon coupling constant and the scaling function defines the coupling constant at each density. In Eq. (11), the parameter α is newly invoked to tune the density dependence in the vector meson couplings, which is relevant to the in-medium effect from the hyperonic sector. This small parameter can be used to adjust the onset density and fractions of hyperons in neutron star matter efficiently. The two free parameters α and $f_{\sigma Y}$ do not change the hyperon potentials at saturation density that are set as the empirical values [13,31,32]

$$U_\Lambda^{(N)} = -30 \text{ MeV} = -U_\Sigma^{(N)}, \qquad U_\Xi^{(N)} = -18 \text{ MeV}. \tag{12}$$

The free-space parameters concerning the hyperons are the same as those in Table 1 of Ref. [13], regardless of the new parameter α. Note that the choice of $U_\Sigma^{(N)}(\rho_0)$ has some arbitrariness for uncertainty [22], and in the present models the Σ hyperons actually do not appear for any repulsive potential. Similar expulsion of Σ hyperons was also revealed in the RMF model GM1 [33].

In the low density region, there are no hyperons and even no muons. The EOS of this density region comprises two pieces: the inner and outer crustal ones. In the inner crust, we adopt a phenomenological EOS $p(r) = a + b\mathcal{E}(r)^{4/3}$ [28,34] with constants a and b being determined by the continuous condition at the core-crust transition density and the density $\rho = 2.57 \times 10^{-4}$ fm^{-3} with the energy density $\mathcal{E} = 0.24$ MeV fm^{-3} and $p = 4.87 \times 10^{-4}$ MeV fm^{-3} which is a point connecting to the outer crust [28,35]. The core-crust transition density ρ_t is here determined as the lowest density of uniform phase by the stability of matter that requires the convex energy against the volume [26,27], and it is 0.0912 and 0.0928 fm^{-3} for SLC and SLCd, respectively. In addition to the above continuous connection, high-order discontinuities may still exist at the core-crust interface. Here, we follow the method in Ref. [9] to deal with the discontinuity in $d\mathcal{E}/dp$ using the Dirac delta function. We have noticed in the work by Piekarewicz *et al.* that a continuous first derivative of pressure is imposed on both interfaces of the inner crust [36]. For the outer crust, we employ the empirical EOS given by Baym *et al.* [35]. Eventually, we adopt the piecewise EOSs for neutron stars with the interfacial matching specified above. It is worth mentioning that Fortin *et al.* studied systematically the uncertainty in the crust thickness and star radius arising from a variety of core-crust EOS matchings [37]. A similar study combined with the GW170817 data was later performed by Ji *et al.* [38]. In this work, we use the same matching scheme to focus on the hyperon contribution concerning the core EOS. For comparison, we also examine the case with the total crustal EOS of Ref. [35] below ρ_t, but find a negligible deviation from the one herein.

III. NUMERICAL RESULTS AND DISCUSSIONS

The discovery of large-mass neutron stars imposed the challenge to the hyperon EOS for neutron stars. In the previous work, the hyperon EOS survives in the large-mass

neutron stars by invoking the density-dependent nucleon-hyperon interactions which allow the hyperons to reside in a shell in the interior of neutron stars [13]. In a multi-messenger era, it is necessary to check whether such a hyperon EOS is compatible with the neutron star tidal deformability extracted from data years ago.

Prior to the discussion of the numerical results, we first interpret the RMF models SLC and SLCd briefly. These two models can reproduce the ground-state properties of finite nuclei fairly well. The only difference of the two models is that the SLCd has a softer symmetry energy at high densities than that of the SLC. The slope parameter L of the symmetry energy at saturation density is 92.3 and 61.5 MeV for the SLC and SLCd, respectively. These values are within or close to some globally averaged values 59 ± 16 MeV [39]. For the slope parameter L, there are also clearly lower ranges either extracted from data [40,41] or obtained from the *ab initio* results of neutron matter [42]. With inclusion of the clearly lower L range, an average of the L values gives a larger range of 58.7 ± 28.1 MeV [43]. Note that the latest measurement of ^{208}Pb neutron skin thickness (0.283 ± 0.071 fm) through the weak-interaction probe [44] would suggest a significantly larger value of $L = 106 \pm 37$ MeV [45]. Very recently, a large span of the L with an upper bound 117 MeV was extracted from the spectra of charged pions [46]. In these cases, the value of $L = 61.5$ MeV with the SLCd would be near the lower bound, and the value 92.3 MeV with the SLC should be still well within the experimental bounds. The neutron skins of ^{208}Pb are 0.21 and 0.17 fm with SLC and SLCd, respectively [25], which agree satisfactorily with values extracted from various experiments. It was found that the symmetry energy is associated with the onset density of hyperons [47]. The soft symmetry energy leads to the smaller neutron chemical potential and consequently the smaller chemical potential of Λ hyperon in chemical equilibrium. The threshold density for the hyperon onset has to be larger so that the required minimum neutron chemical potential can be reached. Thus, we will find that the onset density of hyperons with the SLCd is larger than that with the SLC.

In addition to the symmetry energy, the parameter α in Eq. (11) can also shift the hyperon onset density. The negative value of α ramps up the fraction of the density-independent part of $\Phi_{\omega Y}$, and increases the hyperon chemical potential and consequently the onset density. The positive value of α shifts them on the opposite. In Table I, we present the onset densities of Λ hyperons in different cases. In fact, the hyperon onset density cannot be detected directly and is very different with various interactions in different models, ranging from about $2\rho_0$ to $4\rho_0$. For instance, in usual RMF models, the hyperon onset density locates roughly at twice normal density [47]. In the nonlinear self-interactions involving a vector meson with hidden strangeness, the onset density of hyperons can be as high as $3\rho_0$ arising with a suppressed hyperon fraction [18].

TABLE I. Onset densities of the Λ hyperon for various choices of α and $f_{\sigma\Lambda}$ with the SLC and SLCd. The density is in units of ρ_0 that is 0.16 fm^{-3}.

Model	$f_{\sigma\Lambda}$	$\alpha = 0$	$\alpha = -0.05$	$\alpha = 0.05$
SLC	0.8	2.63	2.70	2.57
	0.9	2.78	2.88	2.69
SLCd	0.8	2.85	2.97	2.77
	0.9	3.06	3.24	2.93

Such a suppression with larger onset densities can also be given by invoking a new boson coupling with hyperons [17]. In Refs. [19,20], hyperons were found to arise above $4\rho_0$ with a rather limited effect on the EOS of neutron star matter. As one can see in Table I, the onset densities in our work are above $2.5\rho_0$, and the small tuning of the parameter α away from naught yields the moderate shift in the onset density within $0.3\rho_0$ that is just moderate, compared to the large diversity presented in the literature.

With the appearance of the hyperons, the EOS becomes softened as naturally given by the stability of matter. This usually results in the considerable reduction of the maximum mass of neutron stars. For instance, with the constant ratio parameters X_{iY} in the present RMF models, the maximum mass of neutron stars is just as high as 1.4 $M_\odot$ [13], which is obviously against the observation of large-mass neutron stars. However, it was revealed [13] that the softening can evolve in density consecutively to a stiffening by invoking the density-dependent hyperonic interaction in terms of the density dependent ratio parameters X_{iY}. More specifically, the occurrence of the stiffening results dominantly from the repulsion provided by the ω meson through the ratio parameter $X_{\omega Y}$. Note that with constant ratio parameters, the problem of the negative nucleon effective mass, encountered at high densities in hyperonized matter, has to be treated by necessarily connecting to the quark matter EOS prior to the occurrence. There is no such problem for the density dependent ratio parameters that are adopted for hyperons in this work. While the stiffening comes up with the suppression of hyperon fractions, the neutron star matter can transit for stability to the normal isospin-asymmetric matter prior to the vanishing of hyperons.

With the EOSs specified, we can carry out the mass-radius relation and tidal deformability parameters of neutron stars. In Fig. 1, the mass-radius trajectories with the SLC and SLCd are plotted for $\alpha = 0.05$ and -0.05. The results with $\alpha = 0$ lie between the two cases and were given in Ref. [13]. We take the curve without hyperons as the fiducial case and measure the relative variation of the trajectories with various parametrizations. As shown in Fig. 1, the parameter α plays a sensitive role in shifting the mass-radius trajectory and radius separation between the normal neutron stars and hyperonized neutron stars. Such an α-induced separation is related to the various hyperon

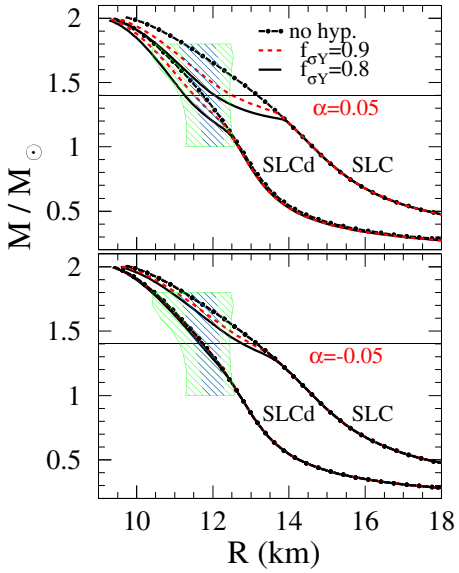

FIG. 1. The mass-radius relation of neutron stars. The parametrizations for various curves are either labeled explicitly or specified in Table I. The star composition of the case without hyperons includes the nucleons, electrons and muons. The hatched areas give the probability distributions with 1σ (blue) and 2σ (green) confidence limits [48].

onset densities shifted by α. Meanwhile, the parameter α also induces the suppression or enhancement of hyperon fractions corresponding to the larger or smaller hyperon onset densities, respectively. As an evidence, we plot in Fig. 2 the total hyperon number fraction as a function of the star mass. We see that the hyperon fraction, which is a ratio of the Λ plus Ξ number over the total baryon number, is generally small. On the other hand, the curves in Fig. 2

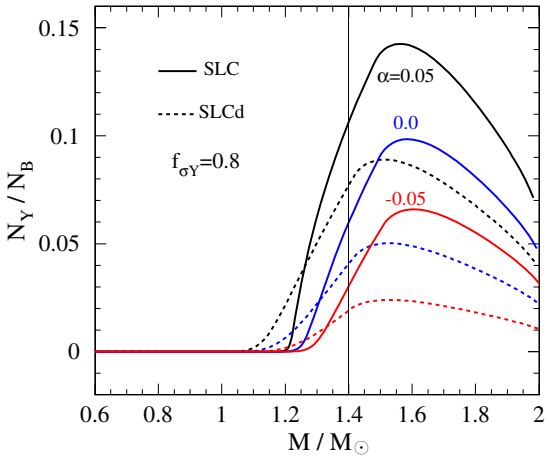

FIG. 2. The hyperon number fraction as a function of star mass. N_Y and N_B are the total hyperon and baryon numbers in the star, respectively. The curves are presented for two models SLC and SLCd with $f_{\sigma Y} = 0.8$ and various α as labeled.

have two more distinct features. The first one is that the significant difference appears in the curves of the SLC and SLCd parametrizations with different peak positions. The smaller fraction with the SLCd is associated with its larger onset density, in contrast to that with the SLC. The peaks in the curves around 1.5 $M_\odot$ with the SLCd and 1.55 $M_\odot$ with the SLC arise as the balance between the heavier star with more hyperons included and the exclusion of the hyperon component in the high density region for the stiffening of the EOS, as mentioned above and referred to Ref. [13] for more details. For instance, an exclusion zone of the hyperons in the 1.5 $M_\odot$ star with all the SLCd parametrizations is a sphere with a radius of about 3 km from the star center, and the hyperon zone extends down to the low density region for about 4 km. For a 1.5 $M_\odot$ star with the SLC, the exclusion zone in about a 1 km radius around the center forms only for the parametrization with $\alpha = 0.05$. Second, a large difference also arises from different α's. With more suppression induced by the parameter α further, the neutron star radius with the SLCd runs almost out of the zone that is sensitive to the hyperon composition, as shown in the lower panel of Fig. 1. As a result, the difference in star radii with the SLC and SLCd reduces clearly by including the hyperon fraction in neutron stars. This clear reduction is eventually attributed to the only difference in two models, namely, the density dependence of the symmetry energy. The softer symmetry energy in the SLCd increases the hyperon onset density and reduces the hyperon fraction significantly, while the SLC with a stiffer symmetry energy gives a smaller onset density with a clearly larger hyperon fraction. The inclusion of hyperons in SLC thus lowers the pressure of matter significantly and results in a clear shrinkage of the star radius, which is consistent with the pressure-radius correlation at intermediate densities ($1.5\rho_0 < \rho < 2$–$3\rho_0$) [26]. Accordingly, an appreciable reduction of the radius difference from two models is observed in Fig. 1.

The Love number k_2, which is carried out together with the mass-radius relation in a set of coupled equations, is shown in Fig. 3. The maximum value of k_2 is situated around 1 $M_\odot$ for the SLC and 0.9 $M_\odot$ for the SLCd, and the difference in k_2 between the two models reaches the maximum around the peak regions. It is found that the difference in k_2 at the given star mass is correlated predominantly with the difference in the star central pressure (or, the central energy density), since the central pressure at the origin serves as the starting point with the largest resistance against the gravity and affects the density profile in the neutron star by integrating the TOV equations and Eq. (4) outwards. For instance, the relative difference in the central energy densities of the two models decreases from about 24% for a 0.91 $M_\odot$ neutron star to about 4% for a 1.3 $M_\odot$ one. As shown in the upper panels in Fig. 3, the difference in the star radii that can be specified by the one in the symmetry energies between the two models just has a

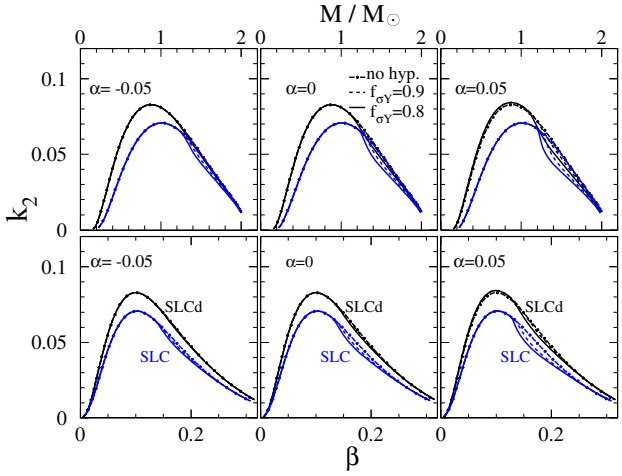

FIG. 3. The Love number as a function of star mass in units of solar mass (upper panels) and compactness $\beta = M/R$ (lower panels) for $\alpha = -0.05$, 0, 0.05. In each panel, the curves subject to the models SLC and SLCd are respectively presented for three cases: without hyperon, $f_{\sigma Y} = 0.8$, and 0.9.

very limited effect on the difference in k_2, especially, for neutron stars with $M > 1.3\ M_\odot$, which is consistent with the result in Ref. [10]. Shown in the lower panels of Fig. 3 is the k_2 versus the compactness parameter β, and the difference in k_2 from the two models at given β can be specified by the different y_R's in Eq. (6) that depend on the radius and central energy density both. It is interesting to see that the hyperon composition, albeit with small fractions in neutron stars, can shift the Love number to some extent, especially in the case of the larger hyperon fraction. This is shown rather clearly in the upper right panel of Fig. 3 with $\alpha = 0.05$ where the hyperon fraction is at the top of three cases as shown in Fig. 2. Here, the relative shift of the Love number between two models arises from a moderate enhancement of the difference in central energy densities and the distinct softening of the pressure in the star interior induced by the hyperons.

Shown in Fig. 4 is the tidal deformability of neutron stars as a function of neutron star mass M. All curves with and without hyperon fractions pass through the experimental constraint extracted for the 1.4 $M_\odot$ neutron star which is 190^{+390}_{-120} [2]. With the inclusion of hyperons, the curves move downwards to the centroid point or further to the lower experimental bound. More displacement of the curves is observed with larger hyperon fractions included. For quantitative clarity, we tabulate the tidal deformability of the 1.4 $M_\odot$ star in Table II. One can see, for instance, that the case with $f_{\sigma\Lambda} = 0.8$ and $\alpha = -0.05$ in the third column where the inclusion of 3% hyperons reduces the tidal deformability from 394.6 to 310.5 by 21.2%, while an inclusion of 10.7% hyperons (in the last column with $\alpha = 0.05$) can reduce the tidal deformability by 42.4%. Such a reduction of tidal deformability can be larger for moderately heavy neutron stars within a rough mass range

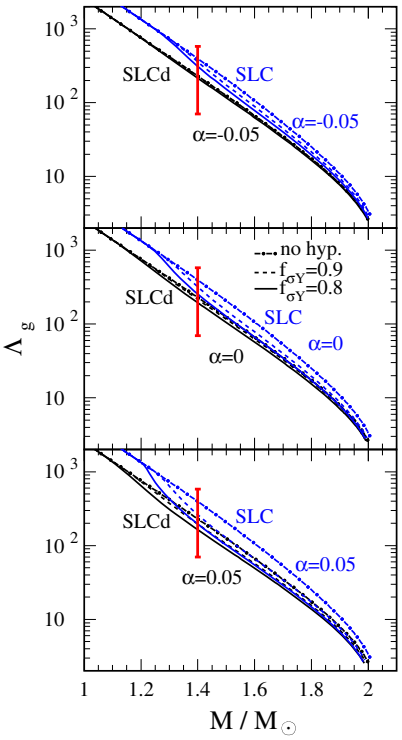

FIG. 4. The tidal deformability as a function of star mass with the same legend as in Fig. 3. The error bar in red is the experimental bounds extracted for the 1.4 $M_\odot$ neutron star [2].

of 1.4 $M_\odot < M < 1.6\ M_\odot$, as can be observed in Fig. 4. Here, we further mention the role of the parameter α. As shown in Table II and Figs. 1 and 4, the roles of the parameters α and $f_{\sigma Y}$ are comparable in adjusting various quantities. We note, however, the small parameter α is more sensitive to adjust the hyperon fractions, see Table II, and can efficiently readjust the effect induced by the parameter $f_{\sigma Y}$, see Fig. 1.

The $\Lambda_g - M$ relation, also see Eq. (7), is advantageous for observing the effect of the radius difference from various models at the given star mass, since in this case the various models may have close Love numbers in a large mass range. This is especially true for models SLC and SLCd that only differ in the density dependence of the symmetry energy and consequently the radius of normal neutron stars with the simplest compositions ($e + \mu + n + p$). Without hyperons, the difference between the Λ_g's from the SLC and SLCd in

TABLE II. The tidal deformability Λ_g of the 1.4 $M_\odot$ star, together with the hyperon number fraction (in percentage) in brackets. Without hyperons, Λ_g is 394.6 and 229.5 with the SLC and SLCd, respectively.

Model	$f_{\sigma\Lambda}$	$\alpha = -0.05$	$\alpha = 0$	$\alpha = 0.05$
SLC	0.8	310.6 (3.06)	255.2 (5.98)	227.4 (10.7)
	0.9	358.8 (1.07)	319.5 (2.65)	260.9 (5.33)
SLCd	0.8	215.0 (1.90)	193.1 (4.07)	163.5 (7.72)
	0.9	226.7 (0.47)	216.4 (1.55)	195.1 (3.61)

the mass region $M > 1.3\ M_\odot$ can be specified by a R^5 dependence as given by Eq. (7), as we see from Fig. 3 that the corresponding Love number nearly overlaps for two models. As the hyperons are included, the Λ_g difference from two models reduces clearly with increasing the hyperon fraction in neutron stars. This reduction is dominated by the correspondingly reduced radius difference from two models in the presence of hyperons, see Fig. 1 and Eq. (7). Second, the Love number undergoes a nonlinear decrease with the increase of the hyperon fraction, see Fig. 3, and this further reduces the difference of Λ_g dominated by the R^5 dependence.

As a result of the reduced Λ_g difference in the models SLC and SLCd that just differ in the density dependence of the symmetry energy, the symmetry energy constraint extracted from the gravitational wave data will be quite different with and without the consideration of hyperon compositions. This is not surprising because the symmetry energy is determined by the in-medium strong interactions and the inclusion of hyperons changes the in-medium effect. As shown in Fig. 4, the Λ_g with the SLC and SLCd come closer with the moderate lowering of the hyperon onset density accompanied by a rise of hyperon fraction. In an extreme case where the Λ_g overlaps, the sensitivity to the symmetry energy vanishes, which means that the experimental bounds of the tidal deformability cannot be employed to constrain the symmetry energy at all. Generally, the inclusion of more hyperons can smear out the constraints on the symmetry energy. The lowest onset density in the present model parametrizations is $2.57\rho_0$. While other models may have the onset density as low as $2\rho_0$ or smaller, even much severer smearing out can be expected to occur for the symmetry energy constraint. On the other hand, were the experimental bounds extracted for heavier stars whose high density content occupies larger fraction, it is advantageous to obtain the constraints for hyperon component in stars, as implied from the results in Fig. 4. For the constraint on the symmetry energy, it favors the experimental bounds of a lower mass star. In order to decouple the effects from the symmetry energy and hyperon component, measurements of multifiducial mass points seem to be necessary in future gravitational wave experiments. At last, we clarify that other non-nucleonic degrees of freedom, in addition to the hyperon component, may also affect the extraction of the density dependence of the symmetry energy. For instance, the inclusion of appropriate dark matter candidates can affect the relation between the mass-radius trajectory of neutron stars and the symmetry energy [49].

IV. SUMMARY

In a multimessenger era, the gravitational wave from neutron star mergers provides a novel probe to the neutron star interior and the relevant nuclear EOS. In this work, we utilize the RMF models with the density-dependent parametrizations to study the neutron star tidal deformability with and without the inclusion of the hyperon fraction. With a small parameter α, the in-medium vector potential for hyperons is adjusted to affect the onset densities and fractions of hyperons sensitively. The decreased (increased) onset density can result in a clear enhancement (suppression) of the hyperon fraction. We have found that the shift of the hyperon fraction with various onset densities (within $0.3\rho_0$) can sensitively affect the star tidal deformability. The present results indicate that the gravitational wave can signal the interior structure and composition of neutron stars. On the other hand, the complication also arises since the constraint on the nuclear symmetry energy, extracted from the gravitational wave signals, would depend on the scenarios of neutron star composition. According to the present results with and without inclusion of hyperons, such a dependence is not negligible. In particular, the difference in symmetry energies signaled by the star tidal deformability may be largely smeared out by the inclusion of hyperons, though the concrete result relies on the values of the free parameters (α and $f_{\sigma Y}$) and is strongly model dependent. To distinguish the effect of the symmetry energy and the hyperon component, the measurement of multifiducial mass points is thus necessary in future gravitational wave experiments.

ACKNOWLEDGMENTS

One of the authors (W. Z. J.) thanks Dr. F. J. Fattoyev for providing us his code which is very helpful to cross-check our calculation of the tidal deformability. The work was supported in part by the National Natural Science Foundation of China under Grant No. 11775049.

[1] B. P. Abbott *et al.* (LIGO Scientific Collaboration and Virgo Collaboration), Phys. Rev. Lett. **119**, 161101 (2017).
[2] B. P. Abbott *et al.* (LIGO Scientific Collaboration and Virgo Collaboration), Phys. Rev. Lett. **121**, 161101 (2018).
[3] F. J. Fattoyev, J. Piekarewicz, and C. J. Horowitz, Phys. Rev. Lett. **120**, 172702 (2018).
[4] S. De, D. Finstad, J. M. Lattimer, D. A. Brown, E. Berger, and C. M. Biwer, Phys. Rev. Lett. **121**, 091102 (2018).

[5] K. Thorne and A. Campolattaro, Astrophys. J. **149**, 591 (1967).
[6] T. Hinderer, Astrophys. J. **677**, 1216 (2008).
[7] T. Damour and A. Nagar, Phys. Rev. D **80**, 084035 (2009).
[8] T. Hinderer, B. D. Lackey, R. N. Lang, and J. S. Read, Phys. Rev. D **81**, 123016 (2010).
[9] S. Postnikov, M. Prakash, and J. M. Lattimer, Phys. Rev. D **82**, 024016 (2010).
[10] F. J. Fattoyev, J. Carvajal, W. G. Newton, and Bao-An Li, Phys. Rev. C **87**, 015806 (2013).
[11] N. B. Zhang, B. A. Li, and J. Xu, Astrophys. J. **859**, 90 (2018).
[12] H. Tong, P. Zhao, and J. Meng, Phys. Rev. C **101**, 035802 (2020).
[13] W. Z. Jiang, B. A. Li, and L. W. Chen, Astrophys. J. **756**, 56 (2012).
[14] J. B. Wei, A. Figura, G. F. Burgio, H. Chen, and H. J. Schulze, J. Phys. G **46**, 034001 (2019).
[15] P. B. Demorest, T. Pennucci, S. M. Ransom, M. S. E. Roberts, and J. W. T. Hessels, Nature (London) **467**, 1081 (2010).
[16] H. T. Cromartie, E. Fonseca, S. M. Ransom, P. B. Demorest *et al.*, Nat. Astron. **4**, 72 (2020).
[17] M. I. Krivoruchenko, F. Simkovic, and A. Faessler, Phys. Rev. D **79**, 125023 (2009).
[18] I. Bednarek, P. Haensel, J. Zdunik, M. Bejger, and R. Manka, Astron. Astrophys. **543**, A157 (2012).
[19] T. Takatsuka, S. Nishizaki, Y. Yamamoto, and R. Tamagaki, Prog. Theor. Phys. Suppl. **146**, 279 (2002).
[20] S. Tsuruta, J. Sadino, A. Kobelski, M. A. Teter, A. C. Liebmann, T. Takatsuka, K. Nomoto, and H. Umeda, Astrophys. J. **691**, 621 (2009).
[21] R. Negreiros, L. Tolos, M. Centelles, A. Ramos, and V. Dexheimer, Astrophys. J. **863**, 104 (2018).
[22] M.Fortin, Adriana R. Raduta, S. Avancini, and C. Providencia, Phys. Rev. D **101**, 034017 (2020).
[23] D. Chatterjee and I. Vidaña, Eur. Phys. J. A **52**, 29 (2016).
[24] W. Z. Jiang, B. A. Li, and L. W. Chen, Phys. Lett. B **653**, 184 (2007).
[25] W. Z. Jiang, B. A. Li, and L. W. Chen, Phys. Rev. C **76**, 054314 (2007).
[26] J. M. Lattimer and M. Prakash, Phys. Rep. **442**, 109 (2007).
[27] S. N. Wei, R. Y. Yang, and W. Z. Jiang, Chin. Phys. C **42**, 054103 (2018).
[28] J. Carriere, C. J. Horowitz, and J. Piekarewicz, Astrophys. J. **593**, 463 (2003).
[29] W. Z. Jiang, Chin. Phys. C **37**, 064101 (2013).
[30] G. E. Brown and M. Rho, Phys. Rep. **396**, 1 (2004); **398**, 301 (2004).
[31] R. Hausmann and W. Weise, Nucl. Phys. **A491**, 598 (1989).
[32] T. Fukuda, A. Higashi, Y. Matsuyama, C. Nagoshi, J. Nakano, M. Sekimoto, P. Tlusty, J. K. Ahn, H. Enyo, H. Funahashi *et al.* (E224 Collaboration), Phys. Rev. C **58**, 1306 (1998).
[33] J. Schaffner-Bielich and A. Gal, Nucl. Phys. **A804**, 309 (2008).
[34] B. Link, R. I. Epstein, and J. M. Lattimer, Phys. Rev. Lett. **83**, 3362 (1999).
[35] G. Baym, C. Pethick, and P. Sutherland, Astrophys. J. **170**, 299 (1971).
[36] J. Piekarewicz and F. J. Fattoyev, Phys. Rev. C **99**, 045802 (2019).
[37] M. Fortin, C. Providencia, Ad. R. Raduta, F. Gulminelli, J. L. Zdunik, P. Haensel, and M. Bejger, Phys. Rev. C **94**, 035804 (2016).
[38] F. Ji, J. Hu, S. Bao, and H. Shen, Phys. Rev. C **100**, 045801 (2019).
[39] B. A. Li and X. Han, Phys. Lett. B **727**, 276 (2013).
[40] J. M. Lattimer and Y. Lim, Astrophys. J. **771**, 51 (2013).
[41] J. M. Lattimer and A. W. Steiner, Eur. Phys. J. A **50**, 40 (2014).
[42] K. Hebeler, J. M. Lattimer, C. J. Pethick, and A. Schwenk, Astrophys. J. **773**, 11 (2013).
[43] M. Oertel, M. Hempel, T. Klähn, and S. Typel, Rev. Mod. Phys. **89**, 015007 (2017).
[44] D. Adhikari, H. Albataineh, D. Androic, K. Anio *et al.*, Phys. Rev. Lett. **126**, 172502 (2021); arXiv:2102.10767v1.
[45] B. T. Reed, F. J. Fattoyev, C. J. Horowitz, and J. Piekarewicz, Phys. Rev. Lett. **126**, 172503 (2021).
[46] J. Estee, W. G. Lynch, C. Y. Tsang, J. Barney, G. Jhang, M. B. Tsang, R. Wang *et al.*, Phys. Rev. Lett. **126**, 162701 (2021).
[47] W. Z. Jiang, Phys. Lett. B **642**, 28 (2006).
[48] A. W. Steiner, J. M. Lattimer, and E. F. Brown, Astrophys. J. **722**, 33 (2010).
[49] Q. F. Xiang, W. Z. Jiang, D. R. Zhang, and R. Y. Yang, Phys. Rev. C **89**, 025803 (2014).